Evolution of the size and shape of 2D nanosheets during ultrasonic fragmentation

Evolution of the size and shape of 2D nanosheets during ultrasonic fragmentation

Andrea Liscio[1,2], Konstantinos Kouroupis-Agalou[1,3], Xavier Diez Betriu[1], Alessandro Kovtun[1], Emanuele Treossi[1], Nicola Maria Pugno[4,5,6], Giovanna De Luca[7,8], Loris Giorgini[3] and Vincenzo Palermo[1]

[1] *Istituto per la Sintesi Organica e la Fotoreattività - Consiglio Nazionale delle Ricerche (ISOF-CNR), via Gobetti 101, 40129 Bologna, Italy*
[2] *Istituto dei Sistemi Complessi - Consiglio Nazionale delle Ricerche (ISC-CNR), via del Fosso del Cavaliere 100, 00133 Roma, Italy*
[3] *Dipartimento di Chimica Industriale 'Toso Montanari', Università di Bologna, viale Risorgimento 4, 40100 Bologna, Italy*
[4] *Italian Space Agency, via del Politecnico snc, 00133 Roma, Italy*
[5] *Laboratory of Bio-inspired & Graphene Nanomechanics, Department of Civil, Environmental and Mechanical Engineering, University of Trento, Trento, Italy*
[6] *School of Engineering and Materials Science, Queen Mary University of London, Mile End Road, E1 4NS London, United Kingdom*
[7] *Dipartimento di Scienze chimiche, biologiche, farmaceutiche e ambientali, Università di Messina, viale Ferdinando Stagno d'Alcontres 31, 98166 Messina, Italy*
[8] *Istituto per i Polimeri Compositi e Biomateriali - Consiglio Nazionale delle Ricerche (IPCB-CNR), P.le E. Fermi 1, 80055 Portici (Napoli) Italy*

Abstract

2-dimensional (2D) nanosheets such as graphene, graphene oxide, boron nitride or transition metal dichalcogenides can be produced on a large scale by exfoliation techniques. The lateral shape of these 2D materials is typically considered random and irregular, and their average size is often estimated using techniques characterized by strong approximations or poor statistical significance. Here we measure in a quantitative, objective way the size and shape of 2D monoatomic nanosheets using a combination of optical, electronic and scanning probe techniques. We measure, one by one, the size and shape of thousands of sheets of graphene oxide as they undergo a standard ultrasonication treatment. Using automatic image processing and statistical modelling we identify two different fragmentation processes in 2D at the nanoscale, related to two populations of nanosheets described by gamma and exponential size distributions respectively. The two populations of sheets coexist during the fragmentation process, each one retaining its average size and shape. Our results explain the size reduction commonly observed in nanosheets upon sonication as an effect of changes in the respective weights of the two populations of nanosheets present in the material.

1. Introduction

In recent years, 2D materials (such as graphene, boron nitride and transition metal dichalcogenides) have attracted increasing attention for a wide range of possible applications, from electronics, to composites, to biology [1, 2].

However, the lack of a clear metrology and quality control is creating confusion among industrial end-users, with many websites and companies selling what should be called graphite powders or thin platelets, rather than graphene. Despite the nomenclature [3] and classification framework [4] that have been proposed for 2D graphene-based materials, a clear agreement on metrology and standards is still missing.

Unlike other nano-materials, graphene can be produced by several methods, either using top-down or bottom-up approaches, leading to a wide range of graphene-based 2D materials with very different quality and cost. For example, high-shear [5] or electrochemical [6] exfoliation techniques, yielding

stable solutions in aqueous and organic solvents, have recently been upscaled from lab to industrial production level.
The final quality of graphene-based solutions and powders depends on a combination of complex processes, including bubble cavitation, shear forces and intercalation, as well as possible chemical oxidation of the pristine graphite. In previous work, we studied the mechanism of how graphene nanosheets detach from bulk graphite upon ultrasonication, comparing this process with (more damaging) chemical or electrochemical exfoliation [7]. After detaching from graphite, the nanosheets continue to be broken and fragmented in solution, due to the presence of ultrasonic waves. An understanding of the physics of such fragmentation processes is important to optimize the production rate of 2D materials with pre-programmed, well-defined and tunable chemico-physical properties.
Standardized approaches to study and describe 2D nanosheets are thus urgently needed, because both fundamental studies and industrial applications require controlled, reproducible properties of the material.

In particular, the size of 2D materials is a fundamental parameter to be estimated because it has an impact on their performance, influencing mechanical and electrical properties in polymer composites [8], charge transport [9], gas permeation in thin films [10] and even biological activity [11].
Here we show that a quantitative study of the nanosheets' size and shape distribution can be done combining statistical, mathematical and physical tools, thus providing detailed information on the physical properties of 2D materials and the dynamics of the mechanisms involved in their production. We describe an analysis technique suitable to characterize large amounts of nanosheets providing robust statistical parameters to describe them. This analysis allows us to define and use a single, scalar quantitative parameter to characterize the areal dispersion of such 2D materials.

Our approach is inspired by the chemists from the first half of the 20th century, who were challenged to find new techniques to produce, characterize and define 1D polymers [12]. One century later, we face similar challenges in producing and characterizing a new class of materials, formed by repeating units not in one but in two dimensions [13], obtained by fragmentation of bulk graphite.
For linear polymeric chains, the molecular weight unambiguously identifies the 1D length of the object. The metrology of 2D materials is however more complex, because exfoliation yields a poly-dispersed range of nanosheets featuring not only a wide range of sizes, but also different shapes. In all works previously published on this topic, the only morphological parameter reported is the lateral size, quantified using two common statistical parameters: arithmetic mean and standard deviation (SD), assuming that the nanosheets' length follows a Gaussian distribution. However, all published experimental data show that, for any given 2D material the size distribution is non-Gaussian, skewed and highly asymmetric [1, 14]. Noteworthy, this skewed distribution is a general statistical feature that appears in almost all areas of science, e.g. the length distribution of polymers, the content of chemical elements in rocks, the abundance of species in biology and the distribution of galaxies in astronomy [15].
Therefore we decided to perform extensive statistical measurements of 2D nanosheets obtained in solution, using microscopic techniques and automatic image processing to extract robust statistical data about the size and shape of these sheets.

We demonstrated the validity of this approach using a standard 2D material as the target system, i.e. graphene oxide (GO) completely exfoliated without any aggregation, featuring more than 99% of monoatomic nanosheets in water [9, 16]. We monitored the evolution of the size of the nanosheets as they underwent a standard ultrasonication treatment from 0 to 100 h. The sheets, spanning a wide size range from 100 μm down to 10 nm (figure 1), were then deposited on ultra-flat silicon substrates and measured using a combination of different microscopy techniques: optical fluorescence microscopy (FM) [16], scanning electron microscopy (SEM) and atomic force microscopy (AFM). The images obtained were then analyzed by an image processing software, which allowed the measurement of the size and 2D shape of all the sheets produced, one by one (See SI). Even though the three

techniques used rely on different physical processes (probing the sample with photons, electrons or a microscopic sharp tip), we could use our analysis procedure in the same way on all collected images. We could, in this way:

- analyze a statistically representative sample of the GO nanosheets, corresponding to more than 2500 sheets for each sample;
- follow the evolution of size and shape distribution of the nanosheets during the fragmentation process;
- fit these data using different mathematical models of dynamic fragmentation [17],
- deduce the underlying fragmentation mechanisms acting on different length scales and
- using the experimental data, select a robust parameter to quantify the heterogeneity of the 2D system studied.

2. Sample preparation and experimental methods

Single-layer GO sheets were obtained by oxidation and exfoliation of graphite using the modified Hummers method [16]. The prepared GO suspensions in water are stable for more than 1 year as confirmed by UV–vis absorption measurements. The fragmentation of GO sheets was obtained by sonicating the suspensions for up to 100 h with an Elmasonic P 70 H ultrasonic cleaning unit (Woutput = 120 W, freq = 37 kHz) (see SI: experimental methods).

AFM was used to monitor the abundance of single layers (>99%) by spin coating the solution (conc = 0.1 g l−1) on an ultra-flat silicon oxide surface. GO sheets were deposited with negligible overlap (<5%) [9] on silicon spanning a wide size range from 100 μm down to 10 nm and examined combining three microscopic techniques: FM, SEM and AFM.

FM is based on the interaction of the nanosheets with fluorescent molecules, as previously described in [16]. SEM and AFM were performed with standard commercial setups (see supporting information).

Image processing and analysis was performed using commercial software (SPIP™ version 6.6.1) able to detect the different sheets by contrast threshold and contour analysis [18] (see SI: Image processing, for details on image flattening and detection algorithm).

The statistical analysis of the discrete variables acquired by the automatic image processing was performed by testing continuous distributions commonly used in fragmentation models: inverse power, log-normal, gamma and exponential functions. The discrimination between different functions was performed by analyzing the distribution itself as well as the corresponding complementary cumulative distribution. The best-fit functions were obtained using the Levenberg–Marquardt algorithm (see SI: Mathematical methods).

3. Results and discussion

3.1. How to describe the morphology of a 2D material

In previous works on exfoliation, the geometrical properties of 2D materials were described only by the lateral size, which was typically obtained by analyzing few tens of sheets with transmission electron microscopy (TEM). From the experimental point of view, this approach is tedious and prone to artifacts, given that the operator arbitrarily chooses the longest axis of the sheet as a definition of its lateral size.

A sheet with a given area can have a square shape or conversely be long and thin. In a similar way, a sheet with a long axis of given length can be square, or elongated, or simply irregular. Thus, 2D objects with variable shape cannot be defined by a single scalar number, neither length nor area. In

general, also the shape of objects plays a crucial role in affecting the rheology of carbon nanoparticle suspensions and nanocomposites [19] or the percolation threshold in networks of shaped objects [20]. We thus describe a GO sheet using different parameters related to their area and their shape. The analysis of the shape of 2D objects is not trivial and several dimensionless parameters are currently used in image analysis to measure shapes [21].

We chose to use the form factor, a standard morphological parameter calculated from the sheet area (A) and perimeter (p), to describe the irregularity of the shape respect to a circle: $\mathrm{FF} = 4\pi A/p^2$. For comparison, we also used another widespread morphological parameter (aspect ratio) which describes the anisotropy of the shape (see supporting info).

Once the shape is fixed, either area or length could be used to describe the object; we chose to report the area distribution rather than the length distribution because measuring the length of an irregular object is somehow arbitrary (the operator has to choose subjectively the longest axis). Conversely, the area of each sheet shall be measured objectively, pixel by pixel, by the software we used [22].

We considered these nanosheets as non-stretchable materials where elastic deformations are negligible. Geometrically, this corresponds to the case in which the surface metric structure is locally Euclidean. Hence, GO sheets can move and bend in solution without any change in their surface area or shape, which are intrinsic properties of the sheet.

3.2. Statistical analysis of the nanosheet average area and size

By analyzing FM, SEM and AFM images, we evaluated the mean values of the chosen morphological parameters for different sonication times. Figure 2 shows the evolution with time of average area and shape (quantified as the form factor defined above). Error bars correspond to the calculated SD. All three techniques gave an excellent agreement, showing that there were none of the systematic errors typical of subjective, manual image analysis, thus demonstrating that different microscopies can be fruitfully combined to probe the sheet populations within a range spanning over six orders of magnitude, from 10^9 to 10^3 nm^2 [21].

A similar trend, but consistently lower $\langle A \rangle$ values, was achieved using a macroscopic averaging technique, dynamic light scattering (DLS). Although DLS provides a fast measurement by probing macroscopic volumes of solution, the data analysis assumes that the measured objects have a 3D spherical shape [23]. A semi-quantitative method to model DLS of 2D nanosheets was previously developed, assuming an infinite rigidity of the dispersed sheets [24]. However, the bending of nanosheets in solution cannot be neglected because folding is energetically more favorable than a perfectly flat sheet [25]. This causes an intrinsic underestimation of the measured size using DLS, especially for large sheets that are more likely to fold. For this reason, the data reported hereafter are obtained from one-by-one analysis of single sheets on substrates, thus avoiding any underestimation due to ensemble averaging typical of DLS or other bulk, macroscopic measurements.

The value $\langle A \rangle \approx 4 \times 108$ nm2 measured for pristine GO at $t = 0$ (corresponding to an average lateral size $\sqrt{A}$ of ~20 µm) decreased to $\langle A \rangle \approx 1.6 \times 105$ nm2 after half an hour of sonication. Thereafter the area continued to slowly decrease, roughly following an exponential trend (dashed line in figure 2(a)). This gradual reduction in size upon sonication is well known, having been commonly observed in all works on the production of 2D materials, and indicates that fragmentation is a scaling process based on random scissions, without variation in the shape of the fragments (see [26, 27], section 5 and figure S12 in supporting info).

However, a change in the shape parameter $\langle \mathrm{FF} \rangle$ is clearly observed in our case after $t = 40$ h (figure 2(b)).

To solve this inconsistency, we studied in detail not only the average area, but also how the sheet areas differ within each sample.

3.3. Analysis of area and size distribution in each sample

The analysis of the area distribution (fA) of each sample (figure 3) revealed more details on the evolution of the material upon fragmentation.

For the initial GO suspension, *f*A was linear in log–log scale (figure 3(a)), indicating a scale-invariant fractal behavior with dimension $D = 1.0 \pm 0.1$ [28]. A scale-invariant area distribution indicates that the initial population can be described in terms of a Smith–Volterra–Cantor set [29] and that the GO exfoliation from bulk graphite proceeds with iterative self-similar steps where the fragmentation mechanism only depends on the details of the chemical exfoliation process, including intercalation of graphite and formation of gas bubbles [7].

After half an hour of sonication the pristine linear trend was still present (figure 3(b)); however, some deviations from linearity were observed for the smaller fragments.

After $t = 2$ h, *f*A changed significantly (figure 3(c)) with the best fit now obtained using a Gamma distribution which becomes predominant after 10 and 20 h (figures 3(d) and (e)). Gamma distributions are typical of random fragmentation models that follow 2D-Voronoi tessellation [26, 30], similar to fragmentation of brittle materials (a.k.a. 'bulk fragmentation'), such as ceramics, glassware and rocks. Such tessellation produces fragments with similar shapes; this process can be explained by mechanical failure of GO sheets due to their structure composed of graphene-like, *sp*2-hybridized patches divided by highly-defective *sp*3 regions [31], where crack propagation shall start [32].

Between 40 and 60 h of sonication (figures 3(f) and (g)) we observed the coexistence of two populations: one consisting of large sheets following a Gamma distribution (called hereafter population *P*G), and the other of small-sized sheets following an exponential distribution (*P*E).

After $t = 100$ h (figure 3(h)) only population *P*E was observed. The exponential distribution indicates the presence of a fragmentation process starting from seed defects on the outer edges of the sheets [33], from which crack lines depart (figure S13). This mechanism can be depicted as some kind of edge (a.k.a. coastal) erosion (see SI).

The time-evolution of average area $\langle A \rangle$ of the two separated populations is summarized in figure 4(a). *P*G sheets fragmented until they reached an asymptotic area $\langle A \rangle$ G = 15 ± 6 × 103 nm2 while *P*Esheets had a smaller area $\langle A \rangle$E = 2 ± 1 × 103 nm2 that was no longer modified by sonication.

This approach, based on the separate analysis of PG and PE, allows us to confirm that the shape of the sheets is fairly constant during the whole fragmentation process. Figure 4(b) shows that the large sheets PG have a quite constant form factor (FF) of 0.45 ± 0.06 while PE are more isotropic, with values of 0.83 ± 0.09.

The form factors, and thus the shape regularity of the two populations remain constant upon fragmentation, in agreement with [26]; thus, the change in $\langle \mathrm{FF} \rangle$ observed in figure 2(b) is not due to a change in the shape of the sheets, but simply to a change in the respective weights of the two populations, with the number of PG decreasing in time due to fragmentation, eventually disappearing and leaving only PE sheets in solution.

To confirm that this behavior was not due to the particular parameter used to measure shape, we performed a similar analysis using another widely used morphological parameter (aspect ratio) which describes the anisotropy of the shape, obtaining the same results (see section 3 and figure S9 in supporting info).

In general, physical models that do not take into account the presence of two distinguished sheet populations failed to describe the fragmentation process. Incoherencies are observed if the sheet area is described in the conventional way, using mean and SD, which cannot account for the contribution of different populations in the sample. These parameters can give a correct statistical description of the sample only when fA is Gaussian. Instead, their use can cause misleading results when comparing distributions with different skew and shape.

Overall, a detailed analysis of how the area and shape of the nanosheets evolved during fragmentation indicates that two different processes acted on different scales. Large sheets PG were broken down by fracture events that divided each sheet into pieces with a comparable shape described by a Gamma distribution and reaching the asymptotic value $\langle A \rangle_G$ corresponding to the ultimate fragments area obtained by 'bulk fragmentation' of the pristine material. Following this stage, a second fragmentation process became relevant, where small pieces were cut from the edges of the larger sheets by an erosion process, creating a new population of objects described by an exponential distribution, having a smaller and constant area $\langle A \rangle_E$. Each populations had a different shape that was not modified by sonication, PE sheets being systematically more isotropic with respect to PG, due to the erosion process.

These results cast new light on the commonly observed fragmentation process of nanosheets with sonication [10, 34]. The decrease of area is not due to a continuous shrinkage that affects all the sheets in the same way, but rather to a change in the ratio of two populations of sheets created by two different physical mechanisms.

We underline that the thickness of GO sheets as well as their chemical composition were constant throughout the entire fragmentation process, as monitored by AFM, x-ray photoemission spectroscopy (XPS) and zeta-potential measurements (figures S10 and S11). The mechanical stress due to the sonication did not create new oxidized defects in the GO sheets and the fractures propagated along already existing defects. The two different mechanisms observed are thus not due to presence of different chemical defects in the initial or later stages, but rather to a change in the physical process of fragmentation while the average sheet size was shrinking.

3.4. Influence of sheet area on mechanical properties

During GO sonication, cavitation shatters the large sheets (PG) creating cracks that propagate from their edges and become unstable, giving rise to side branches, which can merge to form additional (small) fragments, observed as the PE population. The onset of two populations of larger and smaller fragments has previously been observed experimentally in 1D, e.g. in the fragmentation of spaghetti [35] (a problem that fascinated also Nobel laureate R Feynman) and 3D (e.g. in blasting of rocks) but only predicted by theoretical models for 2D systems [36].

The fragmentation action in a typical sonication treatment is based on the implosion of micro-bubbles created by ultrasound cavitation process. Collapsing at super-sonic speed, these bubbles break down the sheets due to shear viscous forces that cause mechanical stress [37]. The asymptotic area of fragments thus generated ($\langle A \rangle_G$) corresponds to the smallest surface on which the viscous stress shall act to break the fragment further.

Thus we used the experimental value found for the smallest average area to estimate the mechanical strength of single nanosheets. In terms of Mott statistical theory [33], we extended a 1D model, previously used for carbon nanotubes [38], to the 2D case (see SI). $\langle A \rangle_G$ and the viscous stress applied by cavitation bubbles were used as input in the model, obtaining a fracture strength of PG sheets of 30 ± 10 GPa, which is in good agreement with estimations from previous modelling [39] and experimental [40] works.

The results presented here demonstrate the complexity of fragmentation in 2D, highlighting that it is not correct to quantify the physical properties of an ensemble of sheets with the most widely-used pair of statistical parameters (i.e. mean and standard deviation). However, the definition of a robust statistical indicator could be useful to describe the uniformity of these materials and to compare them with others.

3.5. A new quantitative approach to measure the heterogeneity of 2D materials in solution

Graphene can be viewed as a polymer consisting of atoms covalently tethered in 2D [41]. Therefore, we propose to extend to 2D objects concepts already developed, one century ago, for 1D polymers. The description of the molecular mass of a polymer is determined by the mass-molar dispersity (ĐM)

[42] which is commonly used for quantitative analysis of static light scattering measurements (SLS), viscometry and size exclusion chromatography [43]. Also known as polydispersity index, ÐMquantifies the variability in length of the polymer chains, and is defined as the weight-averaged molecular weight (Mw) divided by the number-averaged molecular weight (Mn).
Taking into account that the mass of 2D objects is directly proportional to the area (A), we thus extended the validity of ÐM by defining the area dispersity of 2D materials (Ð2D) as:

$$Đ_{2D}=\frac{M_w}{M_n}=\frac{A_w}{A_n}=\frac{\sum f_A\cdot A^2}{\sum f_A\cdot A}\times\frac{N_{TOT}}{\sum f_A\cdot A}=\frac{\langle A^2\rangle}{\langle A\rangle^2} \quad (1)$$

resulting in the mean value of the squared area ($\langle A^2\rangle$) divided by the square of the mean value of the area ($\langle A\rangle$2). Figure 5(a) plots the time evolution of Ð2D of GO sheets during sonication. In the first half hour the dispersity increased indicating a higher heterogeneity of the solution due to the persistence of unbroken pristine material, as discussed before. Afterwards, with continuing sonication Ð2D reduced reaching a value close to 2 ascribable to the PE dispersity.

Finally, we tested the validity of this parameter demonstrating how it can explain some macroscopic property of the material studied. In analogy with 1D polymers, dispersity variation influences the way that light is scattered by 2D objects in solvent. We studied the GO suspension with SLS measurements, which are commonly used to characterize polymers and colloidal solutions. At low particle concentrations and for Rayleigh scattering, the SLS signal is proportional to the ratio between M_w and the *z*-averaged mean-square radius of gyration [44], and can be written as a linear function of $Đ_{2D}$, taking into account equation (1):

$$Y_{SLS}=\alpha+\beta\cdot\frac{M_w}{\langle R_g^2\rangle_z}=\alpha+\beta\cdot\frac{A_n}{\langle R_g^2\rangle_z}\cdot\frac{A_w}{A_n}$$
$$=\alpha+\beta\cdot\frac{A_n}{\langle R_g^2\rangle_z}\cdot Đ_{2D} \quad (2)$$

where α and β represent dimensional and proportional parameters.

The linear trend achieved for $t \geq 20$ h (figure 5(b)) indicates that the ratio $\langle A\rangle/\langle R_g^2\rangle_z$ is constant, confirming the validity of using the $Đ_{2D}$ index for 2D materials. This evidence suggests that the smallest GO sheets produced by long sonication times had no relevant folding in water suspensions, behaving as quasi-planar objects, in agreement with the DLS measurements.

4. Conclusions

Fragmentation can be described as the process of disintegrating an object by multiple fracturing events. The physics of fragmentation is of interest in different fields of science and engineering: materials science, failure analysis and even astronomy. The analysis of the size distribution obtained with a given fragmentation process allows us to understand the underlying physics of that process. As example, using this approach Brown *et al* [45] studied the size distribution of many galaxies, demonstrating that the universe underwent a single fragmentation event separating into protogalactic volumes at a relatively early stage after the Big Bang. In most cases, the study of size distribution is performed on 3D objects (i.e. powders or rocks from mining activities) or on 1D polymers. Here we performed, for the first time, such an analysis on a purely 2D material. While polymers can be

analyzed only at the ensemble level, one of the most striking features of graphene and related 2D materials is that even single sheets can be easily observed with high-throughput microscopy techniques. Thus, they are an ideal material to combine analysis from macro scale to the single sheet, allowing monitoring of chemico-physical processes at the nanoscale.

We underline that it was possible to obtain statistically sound data on all the different sheet populations thanks only to the good quality of the material chosen (GO sheets), whose typical lateral size matches the ideal working range of the selected microscopic techniques very well. Contrary to previous works, the changes in area observed could be ascribed only to 2D fragmentation, not to exfoliation of 3D objects (e.g. graphene multilayers) into 2D nanosheets. This is because the original starting material we chose was already a purely 2D material, thus ruling out any influence of 3D processes on the changes in sheet population.

This approach can be applied to all the 2D materials having topological defects (very few atoms holes), small holes (few nm), fissures, etc., with size significantly smaller than the sheet size. Until defect size is much smaller than sheet size, this will just affect the average fracture strength, but will not change the fragmentation mechanism.

In summary, we described a new protocol for the quantitative analysis at the nano- and micro-scale of fragmentation in two dimensions. The results obtained allow some ambiguities reported in literature to be solved: by showing the coexistence of different GO populations, we demonstrated that the GO suspensions can be described as a blend of large sheets and small debris fragments (similar to fulvic oxides), casting new light on the results recently reported on this topic [46].

The proposed approach, based on measurement and calculation of areal dispersity, builds on methods already well-established for 1D polymers, and could allow a rigorous metrology and a reliable, objective quality control of graphene-like materials for both fundamental and applied research, accelerating the use of these new, exciting materials in industrial applications.

Acknowledgment

We thank Dr Meganne Christian for her comments on the manuscript. The research leading to these results has received funding from the European Union Horizon 2020 Framework Programme under grant agreement n°696656 Graphene Core1 and the EC Marie-Curie ITN-iSwitch (GA no. 642196). NMP is also supported by the European Research Council PoC 2015 "Silkene" No. 693670, by the European Commission H2020 with the Fet Proactive "Neurofibres" No. 732344.

Author contributions

AL and VP conceived the experiments and wrote the manuscript. KKA, XDB, AK, ET and GDL performed sample preparation and characterization. NMP and LG contributed to data analysis. NMP derived the model to quantify the GO mechanical resistance. All authors have given approval to the final version of the manuscript.

References

[1] Coleman J N et al 2011 Science 331 568–71

[2] FerrariAC et al 2015 Nanoscale 7 4598–810 NovoselovKS, Fal'koVI, Colombo L, Gellert PR, Schwab M G and Kim K 2012 Nature 490 192–200

[3] BiancoA et al 2013 Carbon 65 1–6

[4] Wick P et al 2014 Angew. Chem., Int. Ed. 53 7714–8

[5] PatonKR et al 2014 Nat. Mater. 13 624–30

[6] ParvezK, Wu Z-S, LiR, LiuX, Graf R, FengX and MüllenK 2014 J. Am. Chem. Soc. 136 6083–91

[7] Xia ZY, Pezzini S, Treossi E, Giambastiani G, Corticelli F, MorandiV, ZanelliA, BellaniV and PalermoV 2013 Adv. Funct. Mater. 23 4684–93

[8] De S, King P J, Lyons P E, Khan U and Coleman J N 2010 ACS Nano 4 7064–72 VallesC, AbdelkaderA M, YoungRJ and Kinloch IA 2014 Faraday Discuss. 173 379–90

[9] LiscioA, Veronese G P, Treossi E, Suriano F, Rossella F, BellaniV, Rizzoli R, Samori P and PalermoV 2011 J. Mater. Chem. 21 2924–31

[10] Guo F, Silverberg G, Bowers S, Kim S-P, Datta D, ShenoyV and HurtR H 2012 Environ. Sci. Technol. 46 7717–24

[11] RussierJ, Treossi E, ScarsiA, Perrozzi F, Dumortier H, Ottaviano L, Meneghetti M, PalermoV and BiancoA 2013 Nanoscale 5 11234–47

[12] MülhauptR 2004 Angew. Chem., Int. Ed. 43 1054–63

[13] PalermoV 2013 Chem. Commun. 49 2848–57

[14] KouroupisAgalouK, LiscioA, Treossi E, Ortolani L, MorandiV, Pugno N M and PalermoV 2014 Nanoscale 6 5926–33

[15] Limpert E, Stahel W A and Abbt M 2001 Bioscience 51 341–52

[16] Treossi E, Melucci M, LiscioA, Gazzano M, Samori P and PalermoV 2009 J. Am. Chem. Soc. 131 15576

[17] Zhang F 2009 Shock Wave Science and Technology Reference Library (New York: Springer)

[18] LiscioA 2013 Chemphyschem14 1283–92

[19] Cassagnau P 2015 Rheology of Non-Spherical Particle Suspensions ed GAusias (Betlin: Springer) pp 59–75

[20] Mertens S and MooreC 2012 Phys. Rev. E 86 061109

[21] RussJC and DeHoff RT 2000 Practical Stereology 2nd edn (New York: Academic)

[22] GrayA 1993 Modern Differential Geometry of Curves and Surfaces (Boca Raton, FL: CRC Press)

[23] Goncalves G, Vila M, Bdikin I, de AndresA, Emami N, FerreiraRAS, Carlos L D, Gracio J and Marques PAAP 2014 Sci. Rep. 4 6735

[24] Lotya M, RakovichA, Donegan J F and Coleman J N 2013 Nanotechnology 24 265703

[25] Schniepp H C, KudinK N, LiJ L, Prud'hommeRK, CarR, Saville DA and Aksay IA 2008 ACS Nano 2 2577–84

[26] Bertoin J 2001 Probab. Theory Relat. 121 301–18

[27] Krapivsky P L and Bennaim E 1994 Phys. Rev. E 50 3502–7

[28] Turcotte D L 1986 J. Geophys. Res. 91 1921–6

[29] FalconerKJ 2003 Fractal Geometry: Mathematical Foundations and Applications 2nd edn (Chichester: Wiley)

[30] OkabeA, Boots B N and SugiharaK 1992 Spatial Tessellations: Concepts and Applications of Voronoi Diagrams (Chichester: Wiley)

[31] EricksonK, ErniR, Lee Z, Alem N, GannettW and ZettlA 2010 Adv. Mater. 22 4467–72

[32] PalermoV, Kinloch IA, Ligi S and Pugno N M 2016 Adv. Mater. 28 6232–8

[33] Grady D E 2010 Int. J. Fract. 163 85–99

[34] Kucki M et al 2016 Nanoscale 8 8749–60

[35] Audoly B and Neukirch S 2005 Phys. Rev. Lett. 95 095505

[36] Åström JA, Ouchterlony F, LinnaRP and Timonen J 2004 Phys. Rev. Lett. 92 245506

[37] Hennrich F, KrupkeR, ArnoldK, Rojas Stütz JA, Lebedkin S, Koch T, Schimmel T and Kappes M M 2007 J. Phys. Chem. B 111 1932–7

[38] Ahir SV, HuangYY and Terentjev E M 2008 Polymer 49 3841–54

[39] Gomez-NavarroC, WeitzRT, BittnerA M, Scolari M, MewsA, Burghard M and KernK 2007 Nano Lett. 7 3499–503 Suk JW, PinerR D, An J H and Ruoff RS 2010 ACS Nano 4 6557–64

[40] CaoC, Daly M, SinghCV, SunY and Filleter T 2015 Carbon 81 497–504

[41] Kim J, Cote L J and Huang JX 2012 Acc. Chem. Res. 45 1356–64

[42] SteptoRF T 2009 Pure Appl. Chem. 81 351–3

[43] RudinA and Choi P 2013 The Elements of Polymer Science and Engineering 3rd edn (Oxford: Elsevier)

[44] Geiduschek E P and HoltzerA 1958 Adv. Biol. Med. Phys. 6 431–551

[45] BrownWK, KarppRR and Grady D E 1983 Astrophys. Space Sci. 94 401–12

[46] Rodriguez-PastorI, Ramos-Fernandez G, Varela-Rizo H, Terrones M and Martin-Gullon I 2015 Carbon 84 299–309 Rourke J P, Pandey PA, Moore JJ, Bates M, Kinloch IA, YoungRJ and Wilson N R 2011 Angew. Chem., Int. Ed. 50 3173–7

Thomas H R, Day S P, Woodruff WE, VallesC, YoungRJ, Kinloch IA, Morley GW, Hanna JV, Wilson N R and Rourke J P 2013 Chem. Mater. 25 3580–8

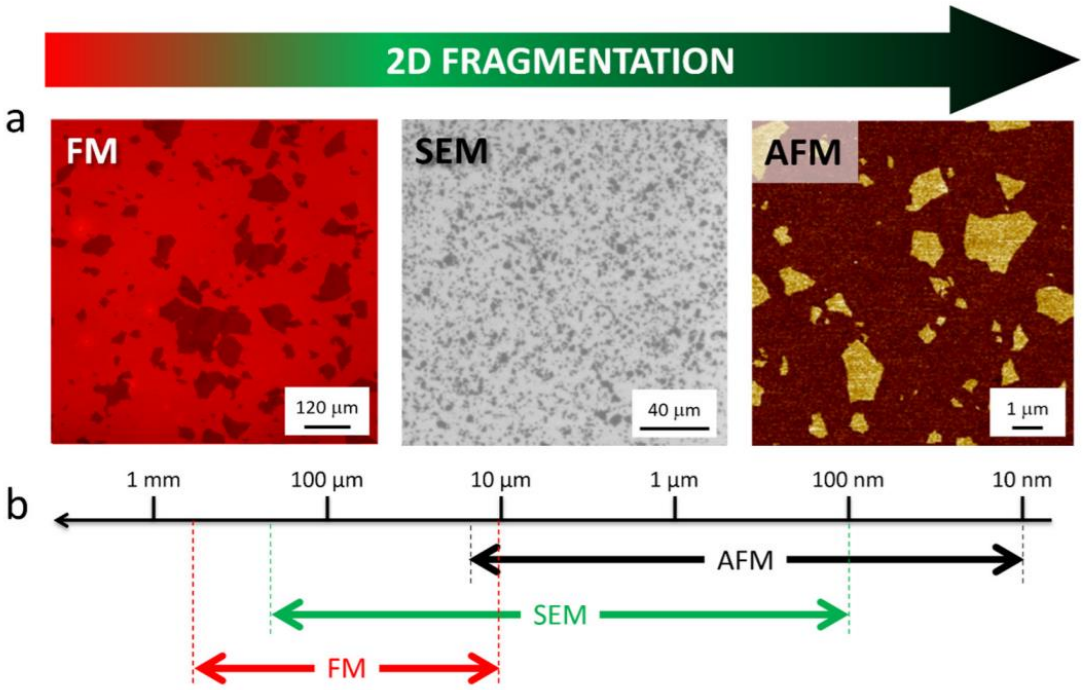

Figure 1. (a) FM, SEM and AFM images of GO sheets deposited on a silicon substrate. Total surface areas sampled using the three techniques: 60 mm^2, 0.1 mm^2 and 0.01 mm^2. (b) A scheme showing the different length-scales explored with the different techniques.

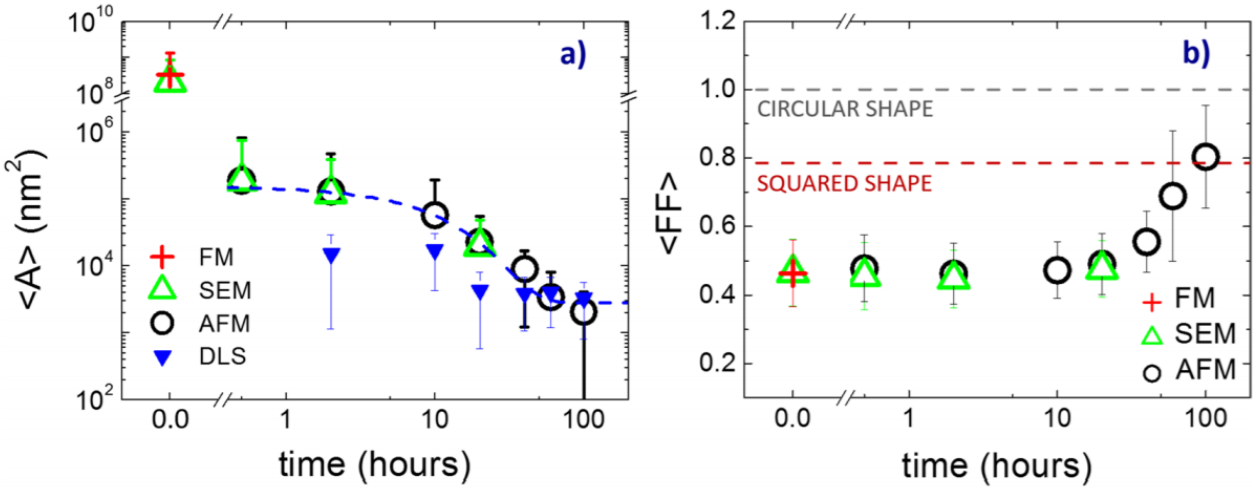

Figure 2. (a) Area and (b) shape evolution of the fragments in function of sonication time directly obtained by (+) FM, (△) SEM, (○) AFM and (▼) DLS. In (a) the blue dashed line shows an exponential fit of the FM, SEM and AFM data points. In (b) the Form factor (FF) is reported, as a measure of shape (see main text). Grey (red) dashed line corresponds to the ideal Form Factor of a circular (square) shaped object.

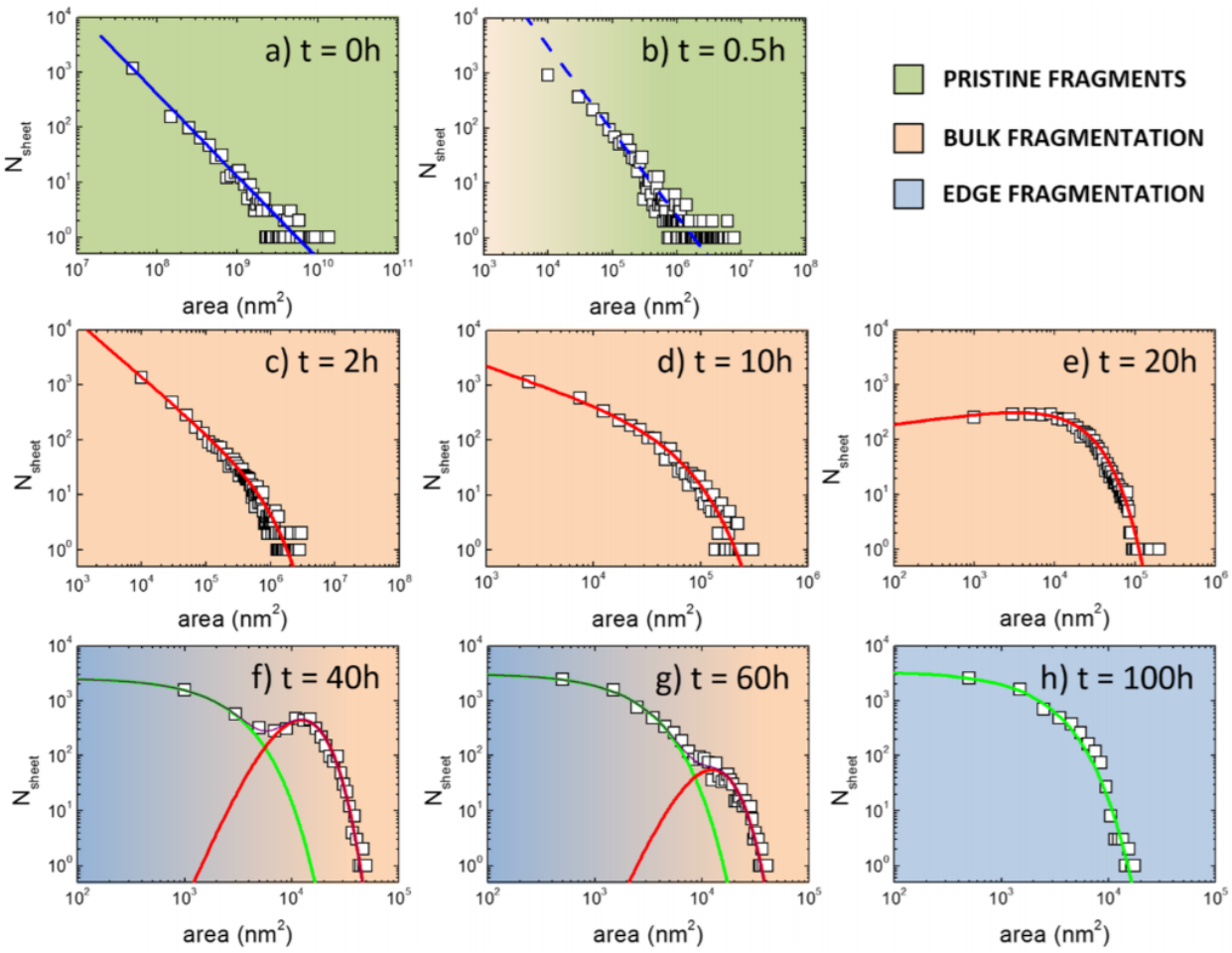

Figure 3. Evolution of size distribution of the 2D nanosheets ((a)–(h)) for different sonication times. The number of sheets (N_{sheet}) versus sheet area is plotted in log–log scale, from 0 h to 100 h. The measured distributions are fitted by: (blue) power law, (red) Gamma and (green) exponential functions. Light green, light yellow and light blue backgrounds indicate different active regimes: pristine fragments, bulk fragmentation and edge fragmentation.

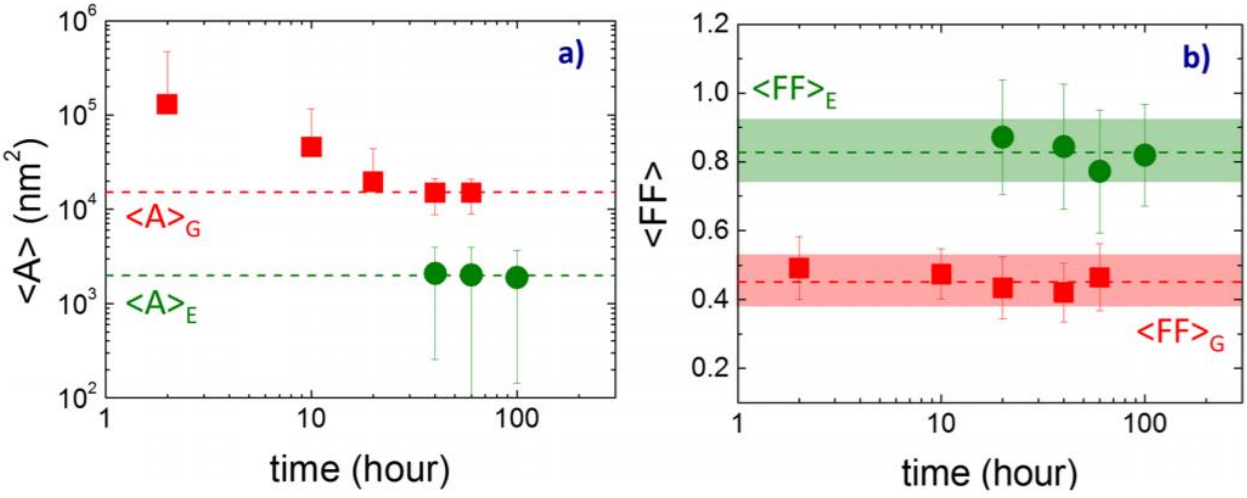

Figure 4. Time-evolution of (a) area and (b) shape, as measured by the form factor (FF) monitoring the two populations: P_G (red squares) and P_E (green circles). $\langle A\rangle_G$ and $\langle A\rangle_E$ are the asymptotic area values of the two populations. Dashed lines correspond to the mean values: $\langle FF\rangle_G$ and $\langle FF\rangle_E$. Shadowed areas are centered to the corresponding average values of the shape parameters (dashed lines) and the widths correspond to twice the standard deviation (=2·SD).

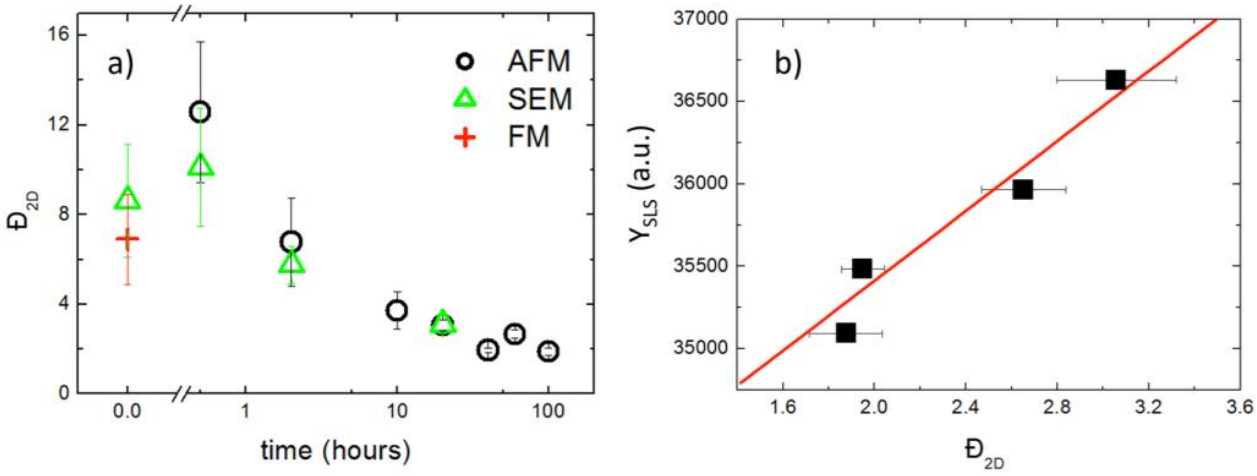

Figure 5. Experimental measurements of 2D areal dispersity index. (a) Time-dependence of areal dispersity $Đ_{2D}$ measured with different techniques. (b) Experimental evidence of the correlation between SLS signal (black squares) and $Đ_{2D}$ for $t > 20$ h. The red line is a linear fit of the experimental data.